Chapter 3
Contaminant Transport Modeling for Homogeneous and Heterogeneous Porous Systems Using MODFLOW Models-Based Scripting Python Package

Abhay Guleria, Sumedha Chakma, and Vijay Pratap Singh

Abstract Contaminant transport modeling for soil column and heterogenous porous system poses a challenge when modeling approach involves non-linear and non-equilibrium sorption models and low permeability porous media (LPPM). Thus, in this chapter, contaminant transport modeling for soil column conditions via 1-D non-linear and non-equilibrium sorption models by means of MODFLOW models-based scripting Python package is presented. Further, contaminant plume evolution dynamics through homogeneous and heterogeneous porous systems, along with sensitivity analysis of flow and transport parameters, is conducted utilizing MT3D-USGS and MODFLOW 6 models. Results from 1-D modeling revealed sorption mass exchange rate as dominating parameter governing concentration at the outlet of soil column. Further, longitudinal dispersivity is observed to be affecting the peak value of concentration for non-equilibrium sorption model. The dominance of molecular diffusion and transverse dispersion on 2-D vertical transport through LPPM is observed from 2-D vertical transport modeling, whereas advection and mechanical dispersion are observed as governing mechanisms in the high hydraulic conductivity zone. Also, the difference in the simulation capabilities of two modeling (i.e., MT3D-USGS and MODFLOW 6) approaches is seen. Overall, this chapter highlighted the influence of sorption isotherm, LPPM, and modeling approach on the contaminant transport modeling.

Keywords Groundwater · Contaminant transport · Heterogeneity · MODFLOW 6 · FloPy

A. Guleria (✉) · S. Chakma · V. P. Singh
Department of Civil Engineering, Indian Institute of Technology Delhi, Hauz Khas, New Delhi 110016, India
e-mail: abhay_guleria@civil.iitd.ac.in

S. Chakma
e-mail: chakma@civil.iitd.ac.in

V. P. Singh
e-mail: ce1180173@iitd.ac.in

P. Shukla et al. (eds.), *Environmental Processes and Management*, Water Science and Technology Library 120, https://doi.org/10.1007/978-3-031-20208-7_3

Abbreviations

C_{im}	Contaminant concentration in the immobile region
K_d	Linear sorption distribution coefficient
K_f	Freundlich equilibrium distribution sorption coefficient
K_l	Langmuir equilibrium constant
$\overline{S}$	Langmuir sorption capacity
α_L	Longitudinal dispersivity
α_{TV}	Traverse vertical dispersivity
θ_{im}	Porosity of the immobile region
ρ_b	Bulk density
ANN	Artificial neural network
BTC	Breakthrough curve
GA	Genetic algorithm
GMS	Groundwater modeling system
GW	Groundwater
LPPM	Low permeability porous media
MADE	Macro dispersion experiment
MOC	Method of characteristic
MODFLOW	Modular three-dimensional finite-difference groundwater flow model
MT3DMS	Modular three-dimensional multispecies transport model
MT3D-USGS	Mass transport in 3-dimensions—U.S. geological survey
MVR	Water mover package
SGeMS	Stanford geostatistical modeling software
TDS	Total dissolved solid
TIAA	Tucson international airport area
C	Dissolved-phase concentration
S	Sorbed concentration
a	Freundlich equilibrium sorption coefficient
t	Time
β	First order sorption mass exchange rate between dissolved and sorbed phases
ξ	First order mass transfer coefficient

3.1 Introduction

Contaminant transport through saturated porous systems with multiple permeability regions is critical when planning remediation activities for any contaminated site (Chapman and Parker 2005; Guo and Brusseau 2017a). Low permeability porous media (LPPM) or aquitard regions behave as a sink during contaminant loading period and as a source, once the contaminating source is removed or isolated

(Chapman and Parker 2005; Rasa et al. 2011; Yang et al. 2017a, b; Guo and Brusseau 2017b). During flushing period or after contaminant source removal, immobile contaminants stored in the dissolved or sorbed phase in the LPPM either diffuse out of these zones due to concentration gradient or cause long plume tailing for a longer duration due to desorption (Brown et al. 2012; Brusseau et al. 2012). Connected networks of preferential flow pathways and mass transfer between high permeability channels and low permeability matrix were observed as governing factors controlling the transport behavior at Macrodispersion Experiment (MADE) site (Zheng et al. 2011). Transverse vertical dispersivity and length of silt/clay layer were found as governing factors of remediation during pump and treat operations while mimicking the field-scale conditions (Carey et al. 2015). Transverse mixing of the conservative contaminant was observed to be governed majorly by a difference in the hydraulic conductivity of matrix and high permeability lenses in comparison with actual pore scale dispersivity (Ballarini et al. 2014). It is observed that the non-ideal transport behavior for large heterogeneous system was mainly associated with mass-transfer mechanisms from dead-end regions, based on the observations of pump and treat operations at Tucson International Airport Area (TIAA) federal Superfund site (Guo and Brusseau 2017a, b). Furthermore, non-ideal mass-removal behavior was observed attributed solely to the back-diffusion from LPPM in the layered or highly heterogeneous subsurface system (Guo et al. 2019). Thus, it can be inferred that the contaminant transport in the presence of LPPM or aquitard regions is complex and needs attention while modeling using any mathematical model.

Several studies were carried out in 2-D and/or 3-D domains in the past that focused on contaminant transport behavior as well as identification of source using an inverse procedure. Singh et al. (2004) solved 2-D groundwater (GW) flow and transport equation using a method of characteristics (MOCs) and used the simulated concentration data to train and test the artificial neural network (ANN). The simulation-based ANN model was developed to identify the unknown pollution source; however, a study was limited to the synthetic case of homogenous aquifer conditions (Singh et al. 2004). A contaminant transport model-based ANN approach was developed too for a scenario in which concentration data for training is partially missing (Singh and Datta 2007). The 2-D GW flow and mass transport equation was solved by MOC. A single soil layer was assumed for an aquifer of size 732 m by 549 m, thus neglecting the impact of heterogeneity (Singh and Datta 2007). Also, a genetic algorithm (GA)-based simulation-optimizer was developed by Singh and Datta (2006) to determine the properties (release period, location, and magnitude of concentration) of unknown GW pollution sources for the simple case (two potential source points and six observation wells) to complex scenario (potential source assumed over some part of aquifer region). USGS-MOC method was used to generate the spatial and temporal concentration data for aquifer of size 1300 m by 800 m and further utilized the simulation data to compute the fitness function value (Singh and Datta 2006). In another study, Visual MODFLOW was used to assess the total dissolved solids (TDS) in the GW in and around dumpsite in Ranipet, Tamilnadu, India (Rao et al. 2011). Observed and model-simulated TDS values were compared to check the accuracy of a numerical model. Similarly, MODFLOW and MT3DMS modules were used

via Visual MODFLOW 4.1 to simulate the TDS in the basaltic terrain of Bagalkot district, Karnataka, India (Rao et al. 2013). Calibration of numerical model was done using observed head data; however, a comparison between model simulations and field observations of TDS was not made (Rao et al. 2013). Different types of ANN models were developed based on the multilevel characterization of breakthrough curve data and highlighted the importance of data for the identification of unknown sources (Singh and Singh 2019). The GMS (version 7.1, 2011, Aquaveo) software was used to solve the GW flow and contaminant transport equations for a synthetic case study representing an aquifer of size 1300 m by 800 m (Singh and Singh 2019). Multilevel BTC characterization performed well as compared to conventional ANN models; however, study was limited to simplistic homogenous aquifer conditions and assumed single fixed lumped value of input parameters for simulations (Singh and Singh 2019).

A multi-layered GW flow and contaminant transport model was conceptualized in GMS v6.5 software to estimate the minimum value of required river flow to enhance the GW quality of the Cauvery river basin, Tamil Nadu (Vetrimurugan et al. 2017). The transport behavior of chloride and nitrate ions from July 2007 to June 2012 was simulated using MT3DMS and MOC-based models, and model calibration was done utilizing observed data (Zheng and Wang 1999; Vetrimurugan et al. 2017). The chloride and nitrate concentration was forecasted for September 2020, assuming various scenarios like water flowing in the river for 30 days in a year, 60 days in a year, and 90 days in a year (Vetrimurugan et al. 2017). Borah and Bhattacharjya (2015) used Groundwater modeling system (GMS 7.1, Aquaveo) software coupled with an ANN-based optimization model to identify the properties of contamination source assuming synthetic example mimicking confined aquifer conditions. Leichombam and Bhattacharjya (2019) implemented MODFLOW to solve GW flow and transport equations and coupled it with an optimization algorithm to determine the unknown locations and flux of contaminant sources. The developed neural network-based models performed well in determining the unknown contamination source, however, limited to simplistic homogeneous aquifer conditions (Singh et al. 2004; Singh and Datta 2007). It is observed that simplistic aquifer conditions, like isotropic, and homogeneous conditions, along with the single lumped value of parameters like porosity and dispersivity, were considered in these field-scale studies (Rao et al. 2011; Borah and Bhattacharjya 2015; Leichombam and Bhattacharjya 2019).

To incorporate the variable nature of flow and transport parameters in the mathematical model, several researchers have developed their in-house code rather than relying on open-source or commercial software. For example, in-house codes of single- and dual-porosity-based contaminant models were developed to simulate contaminant transport in the homogeneous and heterogeneous soil column (Gao et al. 2009; Sharma et al. 2016), and through the stratified porous system (Swami et al. 2016). Variant flow and transport parameters such as dispersion and mass-transfer coefficient were incorporated into the mathematical model to simulate non-Fickian transport behavior in heterogeneous porous systems (Gao et al. 2010; Swami et al. 2018; Guleria et al. 2019, 2020). A two-dimensional contaminant transport problem was solved by a dual porosity-based physical non-equilibrium model, and the impact

of soil type on BTC was studied numerically (Guleria and Chakma 2022). However, it is observed that the above-mentioned studies were not implemented under field-scale conditions (Gao et al. 2009, 2010; Swami et al. 2016, 2018; Sharma et al. 2016; Guleria et al. 2019, 2020). There are few field-scale studies in which heterogeneity of the porous media was considered while developing GW flow and mass transport model. For example, MODFLOW was used to solve the steady-state GW flow equation for a petrochemical plant site of approximately 2 km^2 in Italy, and MODPATH was used to track the trajectory of contaminant plume by assuming different hydraulic conductivity zones (Elshall et al. 2020). A 2-layered aquifer system was considered, in which variation in the hydraulic conductivity (0.43−17.3 m/day) was assigned to the upper confined layer, while 0.01 m/day of hydraulic conductivity was assumed for the bottom confined layer (Elshall et al. 2020). Sathe and Mahanta (2019) assessed GW contamination due to arsenic in Assam, India, by representing porous systems using 2-D lithological and 3-D stratigraphy models, then applied MODFLOW-MT3DMS (3-D software) to simulate field-scale data. The heterogeneous porous system comprised several soil types such as clay, silt, sandy gravel, and boulder with gravel was considered in the modeling; however, model calibration was done by comparing the trend of observed and simulated GW level and ignoring the minimization of residual error (Sathe and Mahanta 2019). It is observed that studies in which MODFLOW-based open-source and/or commercial software was used ignored the variability in the GW flow and transport parameters (Rao et al. 2011; Borah and Bhattacharjya 2015; Leichombam and Bhattacharjya 2019). Most of the studies ignored the impact of LPPM such as silt or clay lenses, on the plume evolution dynamics in the adjoining aquifers (Gao et al. 2010; Rao et al. 2011; Borah and Bhattacharjya 2015; Sharma et al. 2016; Swami et al. 2018; Leichombam and Bhattacharjya 2019; Guleria et al. 2020). Therefore, in this study, the impacts of non-linear sorption processes, LPPM, and stagnant regions on the contaminant transport behavior in the aquifer are studied.

It can be concluded that the contaminant transport dynamics in the presence of immobile regions or LPPM are important to evaluate the risks of possible contaminant rebound during long late time periods. Thus, the main aim of this study is to enhance the understanding of the transport mechanisms in complex heterogeneous systems such as hydraulically coupled aquifers and low permeability porous media (LPPM). Thus, the focus of present chapter is to (i) conduct the contaminant transport simulations for 1-D saturated porous system and compare various non-equilibrium and non-linear sorption models, (ii) analyze the effect of flow and transport parameters on the contaminant plume evolution in the 2-D homogeneous and layered porous systems, and (iii) test the simulation capabilities of MT3D-USGS and MODFLOW 6 models to simulate the contaminant transport behavior in various type of porous systems (i.e., aquifer, aquifer with LPPM, aquifer-aquitard, and aquifer-aquitard with LPPM).

3.2 Methodology

3.2.1 Modeling Approach

The impact of flow and transport through LPPM is studied by developing specialized mathematical modeling approaches such as analytical, semi-analytical, and/or numerical models (Zhan 1998; Zhan et al. 2009; Yang et al. 2015, 2019; Rezaei et al. 2016). Forward and backward diffusive processes in aquitard were considered for an aquitard-aquifer porous system at a macro-scale (Yang et al. 2015). Yang et al. (2019) developed a 1-D analytical solution to analyze the effects of exponential depleting source and back-diffusion from LPPM on long tails in the contaminant breakthrough curves. In the study by Rezaei et al. (2016) and Zhan et al. (2009) for the single-species contaminant transport, flow and transport processes such as advection, vertical diffusion, linear sorption, and first-order irreversible decay were considered for the aquitard region too. However, analytical and semi-analytical solutions are limited to simplistic aquitard-aquifer and/or stratified porous systems. Therefore, graphical user interface-based software is used, developed, and updated to incorporate new challenges to simulate complex contaminant transport phenomena at field-scale conditions. One such popular software is ModelMUSE, which was developed by USGS to solve GW flow and transport problems (Winston 2009). Mescher (2018) used MODFLOW 2005 and MT3D-USGS via ModelMUSE platform to understand the contaminant transport behavior in and around Bordan site, Ontario, Canada. In the study by Mesher 2018, 3 packages of MODFLOW 2005 and five packages of MT3D-USGS models were used to compare the plume evolution of chloride (conservative) and carbon tetrachloride (reactive) contaminants (Mescher 2018). The implementation of the transfer of hydrologic processes among hydrologically connected units was done using water mover package (MVR) within MODFLOW 6 model (Morway et al. 2021). The water transfer between irrigation delivery ditch and multiple cropped areas representing "one-to-many" and runoff transfer from multiple fields routed toward sub-stream representing "many-to-one" connections were shown very well using MVR package (Morway et al. 2021).

In recent years, the Python language has gained acknowledgment in most computational works because of its open-source facility. In the contaminant transport modeling research field, there are few studies in which an open-source MODFLOW-based modeling approach is implemented. For example, Stanford Geostatistical Modeling Software (SGeMS) was utilized to generate the heterogeneous hydraulic conductivity field, and Python scripting package, FloPy, was used to run MODFLOW-based simulations from which flow and transport observed data was further used in parameter estimation (Kheirabadi 2018). A comparison of sequential and combined approaches to calibration was made using PEST++ via a Python programming environment (Kheirabadi 2018). The combined approach performed better than the sequential approach for estimating hydraulic conductivity and porosity, but was observed as time-consuming, complex in usage, and challenging for weight searching process in each run (Kheirabadi 2018). To determine

hydraulic transmissivities via comparison model method for hypothetical aquifer conditions, Comunian and Giudici (2021) conducted simulations using FloPy environment. The Gaussian covariance distribution of transmissivity field was generated using Python package gstools (Müller and Schüler 2019), and further, MODFLOW 6 was used by means of FloPy platform to conduct simulations (Hughes et al. 2017; Langevin et al. 2017). White et al. (2021) developed Python scripting-based tools using FloPy to conduct high-dimensional and geostatistical-based analyses to derive environmental metrics. In another study, a new unstructured finite difference-based gridding approach was developed, and suitability was tested on single and multi-layered porous systems with 4-orders of magnitude variability in the distribution of hydraulic conductivity (Sbai 2020). The technique was ideal for MODFLOW-USG and MODFLOW 6 models and supported the update of the grid from conventional rectilinear to unstructured grids such as Quadtree/Octree Decomposition and Voronoi Tessellations (Sbai 2020). The developed gridding approach was not only confined to geometry-oriented workflow but considered the physics and feedback obtained from the GW flow model (Sbai 2020). Thus, by taking motivation from above-mentioned studies, in this work, an open-source Python scripting package (FloPy) is used to conduct simulations of GW flow and contaminant transport through saturated porous systems (Bakker et al. 2016, 2018). The scripts used in the present study are modified based on the tutorial on FloPy MT3DMS problem (Sudicky 1989; Bakker et al. 2018). Two types of problems were considered (i) 1-D reactive transport modeling through soil column using non-linear and non-equilibrium sorption models and (ii) 2-D vertical conservative transport modeling for homogeneous and heterogeneous aquifer conditions. A detailed description of model parameters and approach adopted is presented in subsequent sections.

3.3 Results and Discussion

3.3.1 Analyzing Non-linear and Non-equilibrium Sorption Isotherms Using 1-D Reactive Transport Modeling

One-dimensional contaminant transport behavior with non-linear (Langmuir and Freundlich) and non-equilibrium sorption isotherms are studied by conducting numerical simulations. The study used FloPy to solve 1-D advection-dispersive transport equation with non-linear equilibrium sorption and non-equilibrium sorption model (Bakker et al. 2016, 2018). The geometrical details mimic the soil column conditions and are based on the example presented in (Zheng and Wang 1999). In this sub-section, MT3DMS and MODFLOW 6 GWT models are used to carry out simulations via FloPy (Bakker et al. 2018); however, results from MODFLOW 6 are shown only. The main focus of these simulations is to analyze the impact of flow and

transport parameters (velocity, sorption mass exchange rate, and longitudinal dispersivity) on reactive transport behavior. Non-equilibrium sorption via MT3DMS-based model is represented as:

$$\rho_b \frac{\partial S}{\partial t} = \beta\left(C - \frac{S}{K_d}\right) \tag{3.1}$$

where S is the sorbed concentration, C is the dissolved-phase concentration, β is the 1st order sorption mass exchange rate between dissolved and sorbed phases, ρ_b is the bulk density, t is the time, and K_d is linear sorption distribution coefficient.

Due to the inability of MODFLOW 6 to model non-equilibrium sorption, a model needs to be approximated by assigning an immobile domain. In this study for a 1-D problem, the value of distribution coefficient is 0.933, which is close to one; thus, the advantage of MODFLOW 6 to approximate non-equilibrium sorption via immobile domain was utilized. It was possible due to the assumption of not considering separate sorption, decay, and production within the immobile domain. The dissolved-phase contaminant mass transfer between the mobile and immobile domain region can be represented as:

$$\theta_{im} \frac{\partial C_{im}}{\partial t} = \xi (C - C_{im}) \tag{3.2}$$

where C_{im} is the contaminant concentration in the immobile region, θ_{im} is the porosity of the immobile region, and ξ is the 1st order mass-transfer coefficient. By assigning immobile domain porosity as bulk density and 1st order mass-transfer coefficient between mobile and immobile regions as 1st order mass-transfer rate for dissolved and sorbed phases, non-equilibrium sorption can be approximated.

Initially, contaminant transport behavior via non-linear sorption (i.e., Freundlich and Langmuir) isotherms are compared for two different down-gradient locations (8 and 16 cm). Secondly, non-equilibrium sorption model is used to simulate the contaminant transport behavior through saturated soil column. Numerical simulations are conducted for 1500 s in which the source is assumed to be present for up to 160 s. The detailed description, such as sorption distribution coefficient and dispersivity, is shown in Table 3.1.

3.3.1.1 Effect of Groundwater Velocity on the Contaminant Transport

The temporal variation of reactive contaminant for Freundlich and Langmuir isotherm model is shown in Fig. 3.1. An early breakthrough point is observed with an increase in velocity ($v = 0.10$ cm/s) for both the observation points (Fig. 3.1a). The peak concentration value is observed at ~ 250 s for $v = 0.10$ cm/s at an 8 cm down-gradient location, whereas for a 16 cm down-gradient location, peak value is observed at ~400 s, indicating the dominance of longitudinal dispersion over source boundary condition at a location away from source. For $v = 0.05$ cm/s at a 16 cm

Table 3.1 Input parameters used for simulation of 1-D column experiment base case

S. No.	Parameter	Value
1	Length	0.16 m (16 cm soil column)
2	Grid spacing	1.6E–03 m (0.16 cm)
3	Pulse duration	160 s
4	Total simulation time	1500 s
5	Dispersivity	0.016 m (1.6 cm)
6	Seepage velocity	1.0E−03 m/s (0.10 cm/s)
7	Porosity	0.32
8	Bulk density	1587 kg/m^3 (1.587 gm/cm^3)
9	Conc. of source fluid	1.0 (unitless)
10	Distribution coefficient	9.33E−04 m^3/kg (0.933 cm^3/gm)
11	Hydraulic conductivity	1.0E−05 m/s (0.001 cm/s)
12	Freundlich equilibrium sorption coefficient (K_f)	$0.3\left(\frac{\mu g}{g}\right) * \left(\frac{l}{mg}\right)^a$
13	Freundlich equilibrium sorption coefficient (a)	0.7 (unitless)
14	Langmuir equilibrium constant (K_l)	$100\left(\frac{l}{mg}\right)$
15	Langmuir sorption capacity ($\overline{S}$)	$0.003\left(\frac{\mu g}{g}\right)$
16	First-order mass-transfer rate between the dissolved aqueous and sorbed phases (β) of non-equilibrium sorption model	0.0/s (case 1)
		10^{-3}/s (case 2)
		10^{-1}/s (case 3)
		10.0 /s (case 4)

down-gradient location, the lowest value of peak concentration is observed at ~850 s among all four scenarios.

In the case of Langmuir sorption model, the rise and fall of breakthrough curve (BTC) is confined to a small-time duration, indicating an early achievement of Langmuir sorption capacity (Fig. 3.1b). A steep slope of rising portion and falling limb of BTC is observed for $v = 0.10$ cm/s as compared to $v = 0.05$ cm/s. The peak concentration of the BTC for the Langmuir model is higher than the Freundlich model for both the GW velocity. In case of Langmuir model, the tailing portion of BTC is smaller as compared to Freundlich model, indicating the attainment of maximum sorption capacity. A large difference in the rising and tailing portion of BTC for different sorption models indicated the significance of choosing the appropriate sorption isotherm as per in situ lab- or field-scale conditions.

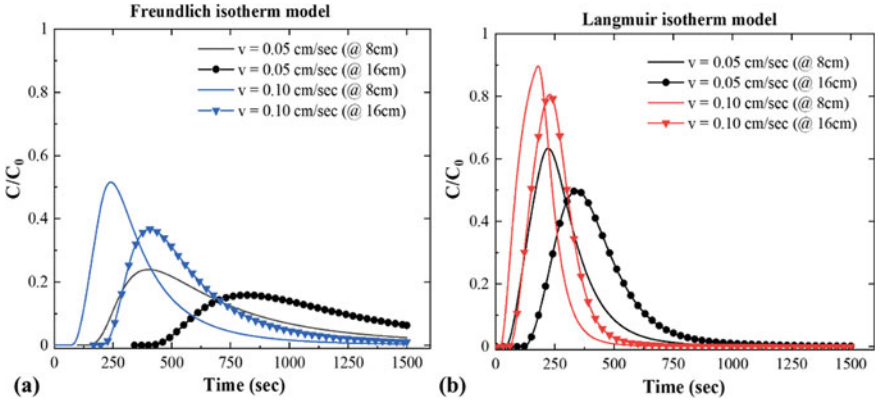

Fig. 3.1 BTC predicted at 8 and 16 cm down-gradient distances by implementing **a** Freundlich and **b** Langmuir isotherm model

3.3.1.2 Effect of Sorption Parameter on the Contaminant Transport Dynamics

The impact of non-equilibrium sorption parameter (β) on the BTC is studied at half- (8 cm) and full (16 cm) soil column length for GW velocity, $v = 0.05$ cm/s (Fig. 3.2). The value of $\beta = 0$ corresponds to a conservative contaminant where no sorption process exists, while a high value of β indicates that the non-equilibrium sorption process occurs at a faster rate so as reached equilibrium state. At 8 cm down-gradient location, the peak concentration value decreases as going from conservative to reactive contaminant ($\beta = 0$/s to $\beta = 10^{-3}$/s). The peak concentration value is observed at ~250 s for lower β values (0/s and 10^{-3}/s) at an 8 cm down-gradient location, while for higher β values (10^{-1}/s and 10/s), the peak value is observed at ~750 s. Also, the magnitude of concentration for higher values of sorption rate is found to be 3–4 times lower than that of lower sorption rate case. It is observed that the concentration value of contaminant decreases with an increase in β value at an 8 cm down-gradient location, showing the mass transfer from solution phase to sorbed phase by sorption processes. The peak value of 0.65 is observed at an 8 cm down-gradient location, while the peak value of 0.50 is observed at a 16 cm down-gradient location for the same value of $\beta = 0$, indicating the impact of longitudinal dispersion process on contaminant transport. Also, it is observed that with an increase in the value of β, the spreading of the BTC increases as observed from BTC at an 8 cm down-gradient location.

The magnitude of concentration ranging from 0.0001 to 0.1 is observed at a 16 cm down-gradient location for higher sorption rates ($\beta = 0.10\ \text{sec}^{-1}$ and $\beta = 10\ \text{sec}^{-1}$), indicating that the peak concentration is not reached yet after 1500 s. It is seen that for higher values of β (e.g., $\beta = 0.10\ \text{sec}^{-1}$ and $\beta = 10\ \text{sec}^{-1}$), the concentration value at both observation points dropped by ~ 5–8 times in comparison with lower values of β (e.g., $\beta = 0.0\ \text{sec}^{-1}$ and $\beta = 0.001\ \text{sec}^{-1}$). Thus, it can be stated that β

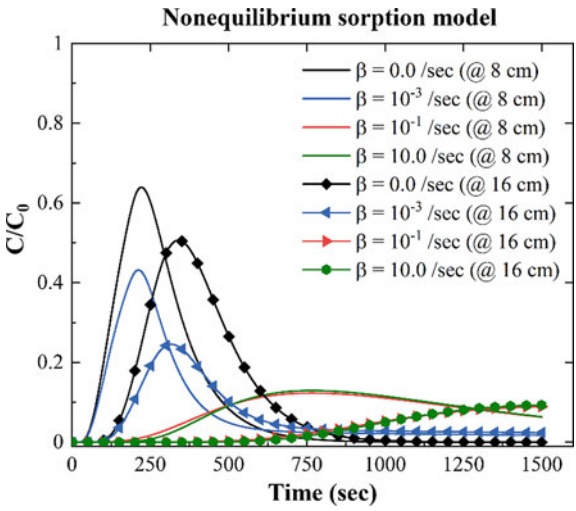

Fig. 3.2 BTC predicted at 8 and 16 cm down-gradient distance for various values of β of non-equilibrium sorption model at groundwater velocity = 0.05 cm/s

is the dominating parameter of non-equilibrium reactive transport model and governs the contaminant transport behavior even for small-scale soil column conditions.

3.3.1.3 Effect of Longitudinal Dispersivity on the BTC

In this sub-section, the effect of longitudinal dispersivity on the prediction of concentration for soil column conditions is shown. Figure 3.3 shows the predicted BTC at a 16 cm down-gradient location for longitudinal dispersivity, $\alpha_L = \frac{L}{10}$ and $\alpha_L = \frac{L}{3}$ via running simulations on MT3DMS (solid lines) and MODFLOW 6 (circles) in FloPy environment. The solid circles from MODFLOW 6 are presented for every 20th-time step. Also, the effect of the non-equilibrium exchange coefficient (β) for two different longitudinal dispersivity values is shown. The results for MODFLOW 6 are shown for every 20th-time step. As observed from BTCs, the results from MODFLOW 6 match well with the MT3DMS simulated BTC. The peak concentration value of 0.80 is observed for $\alpha_L = \frac{L}{10}$ as compared to 0.70 for $\alpha_L = \frac{L}{3}$, depicting the dominance of dispersion processes over advection which eventually causes the reduction in the peak concentration with an increase in longitudinal dispersivity value. The approximate time taken to reach peak value is found as 800 s for $\beta = 0.10$ and $\beta = 10.0$ at longitudinal dispersivity equal to 1/10th of domain length (Fig. 3.3a). However, for longitudinal dispersivity equal to 1/3rd of domain length, the time corresponding to peak concentration is observed to be ~ 550 s (Fig. 3.3b). It shows that the time to reach the peak concentration value and breakthrough time for $\alpha_L = \frac{L}{10}$ are higher than $\alpha_L = \frac{L}{3}$. Thus, it can be stated that with an increase in α_L, the effective dispersion coefficient increases, which causes the early breakthrough time. Overall, it can be observed that the longitudinal dispersivity affects the shape of BTC for higher

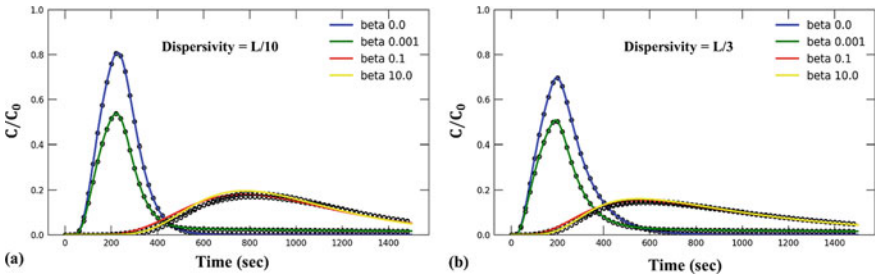

Fig. 3.3 BTC predicted at 16 cm down-gradient distances for **a** dispersivity = 1/10 of domain length and **b** dispersivity = 1/3 of domain length

values of non-equilibrium sorption exchange rate; thus, it needs to be taken care of when modeling the reactive transport behavior even for soil column conditions.

3.3.2 Analyzing the Contaminant Plume Evolution Dynamics for the Homogeneous and Heterogeneous Porous Systems Using 2-D Vertical Transport Model

Sudicky (1989) considered the synthetic field-scale problem to understand contaminant plume dynamics and one of the first problems in which a heterogeneous hydraulic conductivity field was assumed. A highly irregular flow field and a large variation in the longitudinal and transverse dispersivity were considered for testing the simulation capability of flow and transport code to solve real-world problems. By taking motivation from the study by Sudicky (1989), we have studied contaminant transport behavior for the homogeneous, simple layered, and heterogeneous porous system by implementing MT3D-USGS and MODFLOW 6 models in the FloPy environment (Bakker et al. 2016, 2018). Firstly, the impacts of flow and transport parameters such as longitudinal dispersivity, recharge rate, and vertical transverse dispersivity are studied for the homogeneous sand aquifer and simplistic layered porous systems. Then, contaminant plume evolution in various saturated porous systems is compared. Simulation capabilities of MT3D-USGS and MODFLOW 6 to model transport behavior in the layered and heterogeneous porous system are compared too.

A model domain of 250 m in width and 6.75 m on the left side was divided into 27 layers (Fig. 3.4). A steady-state flow in an unconfined aquifer was assumed to model the water table under the impact of recharge. The hydraulic conductivity in both the x- and z-directions was assumed to be equal for any porous media. The contaminant source was assumed to be present at the water table for the first five years of the simulation, and then, a source was removed, and plume evolution was studied for up to 20 years. An initial concentration equal to 0.0 was assumed throughout the domain. The detailed description of flow and transport parameters is shown in

Table 3.2. The XT3D solver was enabled in MODFLOW 6 to compare the simulations from MT3D-USGS and MODFLOW 6 (Bedekar et al. 2016; Hughes et al. 2017; Langevin et al. 2017; Provost et al. 2017).

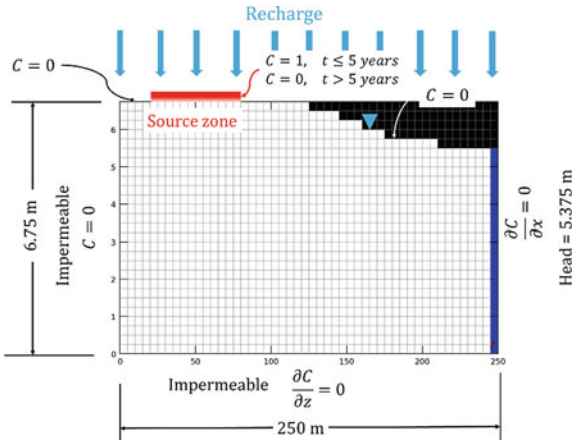

Fig. 3.4 Schematic of model domain used in the study [based on Zheng and Wang (1999)]

Table 3.2 Input parameters used for 2-D vertical transport base case

S. No.	Parameter	Value
1	Width	250 m
2	Depth	6.75 m (left)
3	Grid spacing in x-direction (horizontal)	$\Delta x = 5$ m
4	Grid spacing in z-direction (vertical)	$\Delta z = 0.25$ m
5	Applied recharge rate	10 cm/year (base case)
6	Pulse duration	5 year
7	Total simulation time	20 year
8	Longitudinal dispersivity	0.5 m
9	Traverse vertical dispersivity	0.005 m
10	Porosity	0.32
11	Bulk density	1587 kg/m^3 (1.587 gm/cm^3)
12	Conc. of source fluid	1.0 (unitless)
13	Distribution coefficient	0 m^3/kg (0 cm^3/gm)
14	Hydraulic conductivity (sand)	1.157E−5 m/s (1 m/day)
15	Hydraulic conductivity (clay or low permeability porous media, LPPM)	1.157E−8 m/s (0.001 m/day)
16	Molecular diffusion coefficient	1.34E−9 m^2/s (1.34 × 10^{-5} cm^2/s)

3.3.2.1 Effect of Longitudinal Dispersivity

Figure 3.5 shows the contaminant plume evolution in the homogeneous porous system after 5 and 15 years for different values of longitudinal dispersivity (α_L). Longitudinal dispersivity (α_L) is varied from 0.50 m to 50 m as shown in Fig. 3.5a, c, and e. Contaminant plume front was observed at ~ 100 m in the x-direction and ~2.5 m in the z-direction) away from source zone for $\alpha_L = 0.50$ m in 5th year (Fig. 3.5a), whereas for $\alpha_L = 50$ m, the plume front stretched along the x-direction and was observed near 200 m in the x-direction and ~5 m in the z-direction away from source zone (Fig. 3.5e). The maximum value of C/C_0 equal to 1 is observed near the water table in the source zone in 5th year. However, after source removal, the maximum value of C/C_0 decreases significantly, as observed at 15th-year time level. The contaminant plume shape varied significantly for different values of longitudinal dispersivity, as seen in Fig. 3.5b, d, and f. The peak concentration value of 0.50 is observed for $\alpha_L = 0.50$ m after 15 years in comparison with 0.15 value observed for $\alpha_L = 50$ m, indicating the effect of longitudinal dispersivity on the magnitude and shape of the contaminant plume.

Figure 3.6 shows the contaminant plume dynamics for a simplistic layered porous system in which one layer is kept with a hydraulic conductivity of 1.0 m/day while hydraulic conductivity of another layer is kept at 10^{-3} m/day. It is observed that the contaminant plume shape remains approximately the same for the homogeneous and layered porous system for $\alpha_L = 0.50$ m in 5th year (Figs. 3.5a and 3.6a). For $\alpha_L = 5$ m, the distribution of contaminant plume varied significantly when the plume front entered the LPPM zone. In the LPPM zone, the contour line of contaminant plume becomes perpendicular to bedding plane, indicating the dominance of transverse dispersion over other transport processes. More prominently, the impact of molecular diffusion on plume evolution is observed in the LPPM zone for all the

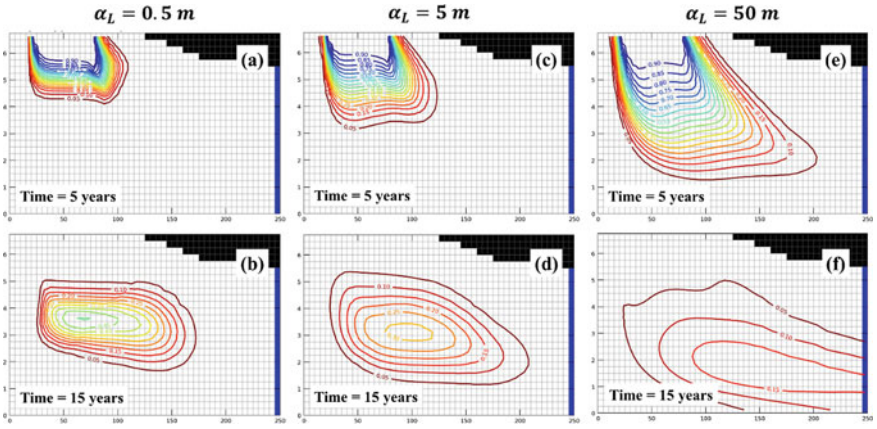

Fig. 3.5 Contaminant plume evolution in the homogeneous porous system for different longitudinal dispersivity values **a, b** $\alpha_L = 0.50$ m, **c, d** $\alpha_L = 5$ m, and **e, f** $\alpha_L = 50$ m

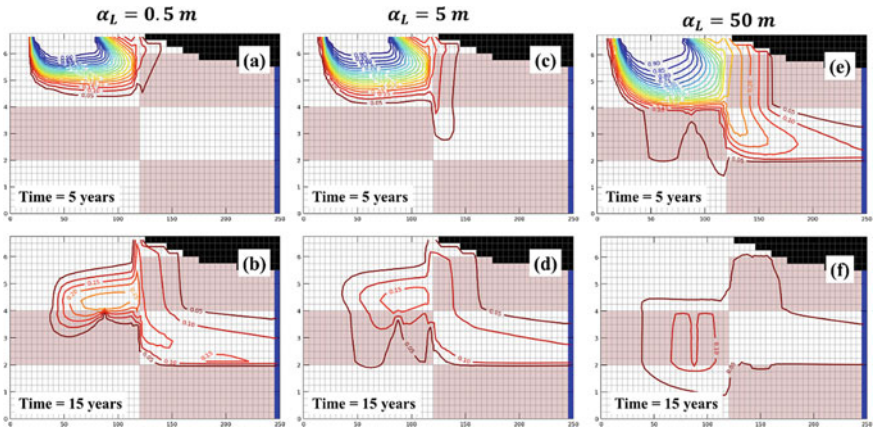

Fig. 3.6 Contaminant plume evolution in the layered porous system for different longitudinal dispersivity values **a, b** $\alpha_L = 0.50$ m, **c, d** $\alpha_L = 5$ m, and **e, f** $\alpha_L = 50$ m

values of longitudinal dispersivity. After source removal, in the 15th year, it is seen that the contaminant transport in the high hydraulic conductivity zone is governed by advection and mechanical dispersion, while contaminant transport in the LPPM zone is dominated by diffusion in the transverse direction. A decrease in the peak concentration value is observed with an increase in longitudinal dispersivity from $\alpha_L = 0.50$ m to $\alpha_L = 50$ m (Fig. 3.6b−f).

3.3.2.2 Effect of Recharge Rate

Recharge rate is one of the important parameters governing the dilution of contaminant plume. In this sub-section, the effects of three different values of recharge rates, viz. 10, 20 and 50 cm/year, on the contaminant transport behavior are analyzed in the presence and absence of contaminant source. The contaminant plume front in 5th year is observed at 120 m from left side of numerical domain for a 10 cm/year recharge rate (Fig. 3.7a), while for a 20 cm/year recharge rate, the plume front with 0.05 concentration contour line reaches at ~140 m distance after five years. For 50 cm/year of recharge rate, the plume front reaches 250 m distance in 5th year, showing an increase in migration rate of contaminant plume with an increase in recharge rate from 10 cm/year to 50 cm/year for a homogeneous porous system (Fig. 3.7c). After the source removal, the shape of contaminant plume is observed as different for different recharge rates. The contaminant plume in 10th year stretches from 25 to 125 m distance in the longitudinal direction for a 10 cm/year recharge rate; however, for a 20 cm/year recharge rate, the contaminant plume stretches from 25 to 225 m in the x-direction. A significant difference in the contaminant plume distribution is observed at 15th-year time level for different values of recharge rate. The peak concentration contour line of 0.50 is observed for a 10 cm/year recharge

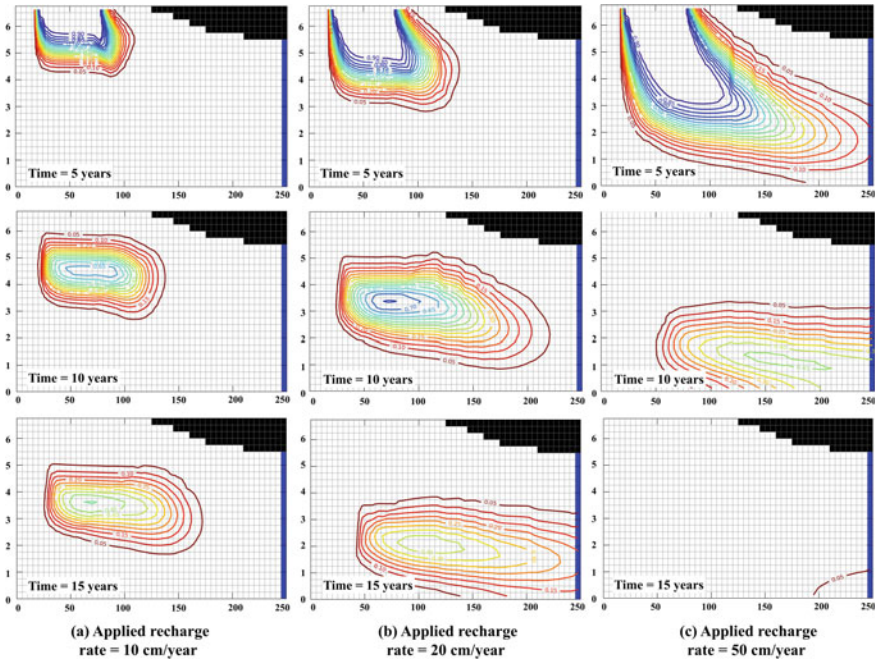

Fig. 3.7 Comparison of contaminant plume evolution with different recharge rates in the homogeneous porous system (MODFLOW 6)

rate, while for a 20 cm/year recharge rate, the peak contour line drops to 0.40, and plume moves to the right-bottom side of the domain. At 50 cm/year recharge rate, the contour line of 0.05 is observed at a right-bottom corner portion of the numerical domain depicting the complete dilution of contaminant plume at 15th year for 50 cm/year recharge rate. It is observed from Fig. 3.7 that the center of mass of plume moves diagonally, and dilution of contaminant plume becomes faster with an increase in applied recharge rate.

Figure 3.8 represents the contaminant plume evolution in the simplistic layered porous system for different values of applied recharge rates. The contaminant plume front at 5th year is observed at 140 m distance from left side of numerical domain for 10 cm/year recharge rate; however, for 20 cm/year recharge rate, the contaminant plume with 0.05 contour line is observed at 215 m. Similarly, highly non-uniform contaminant distribution is observed for a recharge rate of 50 cm/year in 5th year. It is interesting to see that the contaminant contour line becomes perpendicular to LPPM bedding plane at upper one-third portion of a numerical domain and then stretches along the x-direction when enters the aquifer region. The dominance of advection and dispersion processes increases with an increase in the applied recharge rate. However, in the LPPM zone, the impact of recharge rate is not as prominent as in the sand layer. It is observed that the contaminant plume distribution varied significantly for different recharge rates in 10th and 15th years during source unloading period.

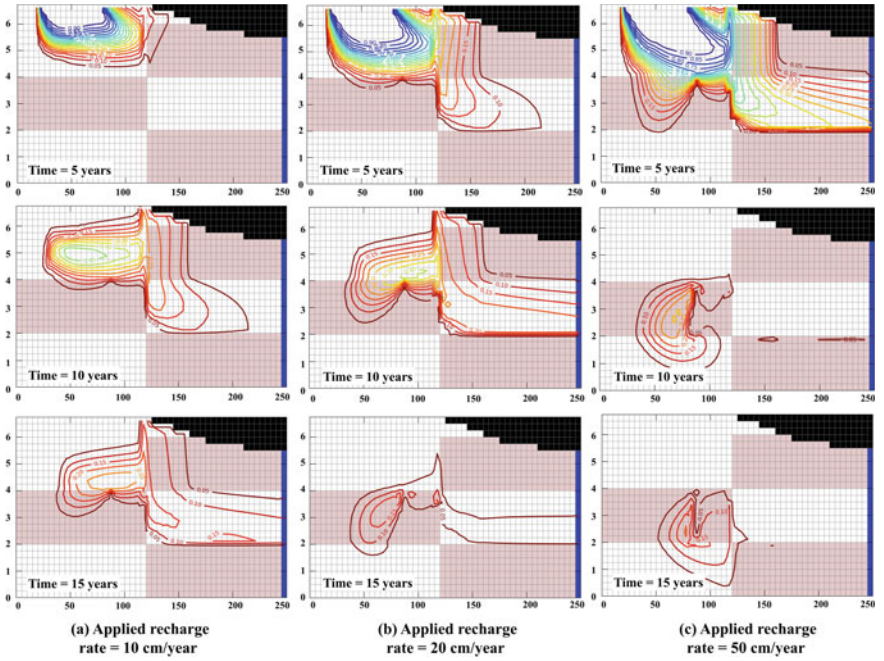

Fig. 3.8 Comparison of contaminant plume dynamics in the layered porous system with different recharge rates (MODFLOW 6)

The peak concentration contour line of 0.15 is observed in the LPPM regions for 20 and 50 cm/year recharge rates, whereas a negligible concentration value is observed in the sand (aquifer) layer. This shows the impact of back-diffusion at later transport times at higher recharge rates, which highlighted the significance of LPPM on contaminant distribution in the adjoining aquifer regions. Also, a significant difference in the plume evolution dynamics is observed for homogeneous and simplistic layered porous systems (Figs. 3.7 and 3.8).

3.3.2.3 Effect of Vertical Transverse Dispersivity

Figure 3.9 shows the contaminant plume evolution in the simplistic layered porous system for different values of α_{TV}/α_L, representing the impact of vertical transverse dispersivity on contaminant transport. The contaminant plume front representing 0.05 contour line reaches ~4.25 m from bottom of the numerical domain for $\frac{\alpha_{TV}}{\alpha_L} = 0.01$ in 5th year; however, for $\frac{\alpha_{TV}}{\alpha_L} = 0.10$, the plume front reaches at 3.5 m level. Thus, it can be stated that the spreading of contaminant plume along a vertical direction increases with an increase in α_{TV}/α_L ratio. After the source removal, the impact of diffusive process on the contaminant distribution in the LPPM zone is seen at 10th year (Fig. 3.9b) and 15th-year time level (Fig. 3.9c). For $\frac{\alpha_{TV}}{\alpha_L} = 0.01$, the effective

hydrodynamic dispersion term in the transverse direction is dominated equally by molecular diffusion and mechanical dispersion term. The peak contour level of 0.45 is observed for $\frac{\alpha_{TV}}{\alpha_L} = 0.01$ in 10th year (Fig. 3.9b), while for $\frac{\alpha_{TV}}{\alpha_L} = 0.1$ ratio, the peak contour level drops to 0.25, showing the dilution of contaminant concentration at higher values of transverse dispersivity (Fig. 3.9e).

For $\frac{\alpha_{TV}}{\alpha_L} = 0.1$, the effective hydrodynamic dispersion term in the transverse direction is dominated by mechanical dispersion term. Also, it is observed that when contaminant plume front enters the LPPM zone at 10th year for $\frac{\alpha_{TV}}{\alpha_L} = 0.1$ value, then plume does not spread along the longitudinal direction, instead enters directly into LPPM zone (Fig. 3.9e). At the 15th-year time level, the peak concentration contour line of 0.25 is observed for $\frac{\alpha_{TV}}{\alpha_L} = 0.01$ with contour intervals at close distances;

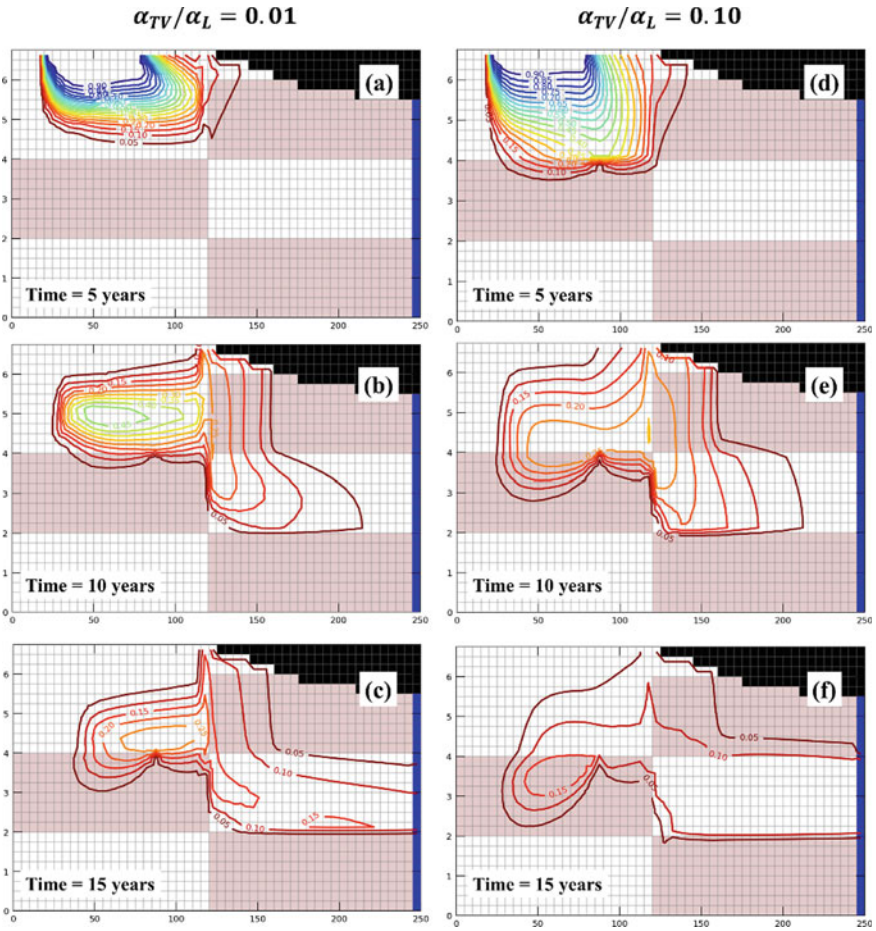

Fig. 3.9 Contaminant plume evolution in the layered porous system for the different ratio of transverse to longitudinal dispersivity **a**, **b**, and **c** $\frac{\alpha_{TV}}{\alpha_L} = 0.01$ and **d**, **e**, and **f** $\frac{\alpha_{TV}}{\alpha_L} = 0.10$

however, for $\frac{\alpha_{TV}}{\alpha_L} = 0.1$, the peak contour value drops to 0.15. It indicates that lumping of dispersion terms at higher values of vertical transverse dispersivity and plume evolution is dominated by advection and mechanical dispersion processes, which further lead to a decrease in the magnitude of contaminant concentration with an increase in α_{TV}/α_L ratio (Fig. 3.9f). Interestingly, the peak concentration contour is observed in the LPPM region, and very low concentration values are observed in the adjoining aquifer region, depicting the effect of back-diffusion from LPPM at very late transport times.

3.3.2.4 Comparison of Simulation Capabilities of MT3D-USGS and MODFLOW 6

In this sub-section, the impact of mathematical modeling choice on predicting contaminant concentration in the aquifer-aquitard system with LPPM is studied. The contaminant plume predicted via MT3D-USGS model for 5th, 10th, and 15th-year time level is shown in Fig. 3.10a, c, and e, while contaminant plume prediction using MODFLOW 6 in 5th, 10th, and 15th years is shown in Fig. 3.10b, d and f. It is observed that, during source loading period (at 5th year), the contaminant plume predicted by both the models is approximately the same (Fig. 3.10a and b). It may be due to the dominance of source concentration over GW flow and transport processes during early transport time. However, after the source isolation/removal, a significant difference in the contaminant plume distribution is observed in the 10th year and 15th year. The shape of contaminant plume lumps out when predicted via MT3D-USGS, while the MODFLOW 6 considers the GW flow and transport mechanisms at the microscale. It is observed that the contaminant plume shape predicted for 10th year (Fig. 3.10d) and 15th year (Fig. 3.10f) using MODFLOW 6 is highly asymmetrical, indicating that the GW flow and transport processes through LPPM are considered in the model. In contrast, MT3D-USGS lumps out the GW flow and transport processes through LPPM. The difference in the contaminant plume shape via different modeling frameworks highlights the impact of modeling choice. Based on the results highlighted above, it can be stated that MODFLOW 6-based modeling framework mimics the realistic contaminant transport scenario effectively as compared to MT3D-USGS model in FloPy.

3.3.2.5 Comparison of Contaminant Plume Evolution Dynamics for Homogeneous and Heterogeneous Porous Systems

Asymmetrical contaminant transport behavior is observed for a porous system comprising contrasting hydraulic conductivity regions, specifically after source removal/isolation. Based on observations obtained in previous simulations, in this sub-section, contaminant plume evolution is analyzed for different arrangements of saturated porous systems. Figure 3.11 shows the contaminant plume in 10th year for different types of saturated porous systems, viz. aquifer, aquifer with LPPM,

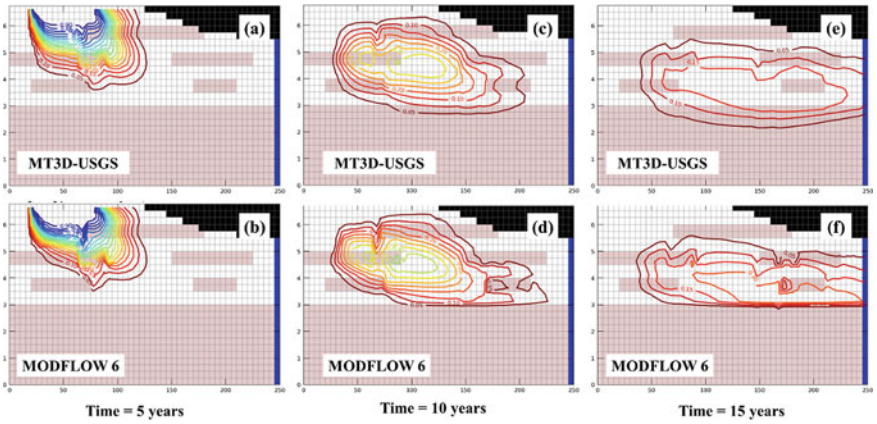

Fig. 3.10 Comparison of contaminant plume distribution in the aquifer-aquitard system with LPPM zone simulated via **a**, **c**, and **e** MT3D-USGS, and **b**, **d**, and **f** MODFLOW 6 models in FloPy environment

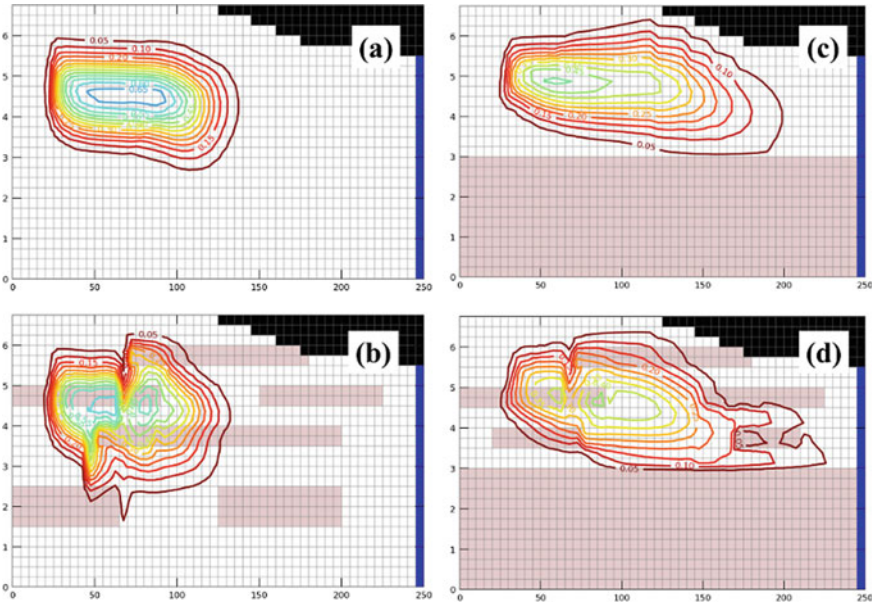

Fig. 3.11 Contaminant plume distribution after 10 years (source removal) in different types of porous system **a** aquifer, **b** aquifer with LPPM, **c** aquifer-aquitard, and **d** aquifer-aquitard with LPPM

aquifer-aquitard, and aquifer-aquitard with LPPM. The uniform distribution with a peak concentration contour of 0.65 is observed for aquifer-type porous systems (Fig. 3.11a). It is observed that the plume stretches along x-direction dominantly for aquifer system; however, for aquifer with LPPM, the plume stretches asymmetrically along x- and z-direction equally (Fig. 3.11b). Even the dominating effect of molecular diffusion and, subsequently, transverse dispersion on plume movement is seen for aquifers with LPPM, which is undermined in the case of homogeneous aquifer system. In the case of aquifer-aquitard system, the contaminant plume behaves same as aquifer system until the plume front reaches the aquitard layer. As plume front reaches the aquitard region, the contaminant plume gets elongated along the x-direction, showing that the aquitard layer does not allow the contaminant to penetrate, which might be due to very low flow velocities in aquitard layer (Fig. 3.11c). In the case of an aquifer-aquitard system with LPPM, a highly asymmetrical contaminant plume distribution is observed in the 10th year. The peak concentration contour level of 0.45 is observed, showing a decrease in contaminant movement in the aquifer-aquitard system with LPPM as compared to homogeneous aquifer system. The influence of molecular diffusion in the LPPM region is observed, while advective and dispersive fluxes dominate the contaminant transport in the high hydraulic conductivity (aquifer) region (Fig. 3.11d).

Figure 3.12 shows the contaminant plume in 15th year for different types of saturated porous systems. The overall transport behavior for various types of porous systems in 15th year is same as in the 10th year. The peak value of concentration decreases with an increase in time, which represents the dilution of concentration by dispersion processes. For aquifer-aquitard system, the peak concentration contour level of 0.25 is observed with contaminant plume stretched along the x-direction dominantly in comparison with z-direction after 15 years (Fig. 3.11c). The concentration contour level is observed as parallel to the aquitard layer and does not allow contaminant to penetrate. The zones of higher values of contaminant concentrations are observed in the high hydraulic conductivity regions even after ten years of source isolation/removal; however, small patches of high concentration values are observed in the LPPM regions. It shows that the LPPM regions act as a contaminant source at later transport times (Fig. 3.12b and d).

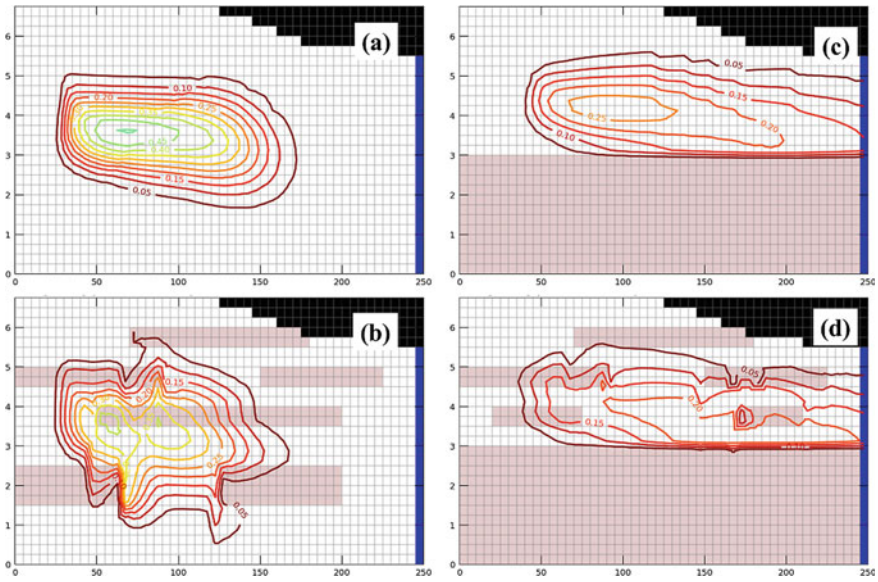

Fig. 3.12 Contaminant plume distribution after 15 years (source removal) in different types of porous system **a** aquifer, **b** aquifer with LPPM, **c** aquifer-aquitard, and **d** aquifer-aquitard with LPPM

3.4 Conclusion

This chapter presents the modeling of contaminant transport via 1-D non-linear and non-equilibrium sorption models. Secondly, a comparison of transport behavior for homogeneous and heterogeneous porous systems is presented, along with the sensitivity of model parameters. Finally, the simulation capabilities of MT3D-USGS and MODFLOW 6 models to simulate the contaminant transport behavior in various types of porous systems (i.e., aquifer, aquifer with LPPM, aquifer-aquitard, and aquifer-aquitard with LPPM) are highlighted. The results from non-equilibrium sorption model indicate that the concentration at a down-gradient location for soil column conditions decreases with an increase in sorption mass exchange rate, indicating it as dominating parameter of non-equilibrium reactive transport model. A significant impact of longitudinal dispersivity on the shape of BTC is seen for higher values of non-equilibrium sorption exchange rate. The results from 2-D vertical transport modeling depict the impact of LPPM on contaminant plume evolution. The dominance of molecular diffusion and, subsequently, transverse dispersion on contaminant transport behavior through LPPM is observed. At the same time, advection and mechanical dispersion processes are observed to be governing the transport behavior in the high hydraulic conductivity (aquifer) zone. Also, it is observed that the MODFLOW 6 considers the microscale processes through LPPM, whereas MT3D-USGS ignored these processes and lumped them into macro dispersion

coefficient while modeling transport behavior in LPPM regions. The simulations depict the LPPM regions as source terms at later transport times after source isolation/removal and sink terms during the loading period. However, this chapter is limited to dissolved species transport problems in the saturated porous system. Flow and transport modeling of nonaqueous phase liquids (LNAPLs and DNAPLs) in unsaturated porous media can be conducted in FloPy environment to give a broader aspect to the applications of Python scripting-based package.

References

Bakker M, Post V, Langevin CD et al (2016) Scripting MODFLOW model development using python and FloPy. Groundwater 54:733–739. https://doi.org/10.1111/gwat.12413

Bakker M, White JT, Langevin CD, et al (2018) FloPy v3.2.9: U.S. geological survey software release. pp 12

Ballarini E, Bauer S, Eberhardt C, Beyer C (2014) Evaluation of the role of heterogeneities on transverse mixing in bench-scale tank experiments by numerical modeling. Groundwater 52:368–377. https://doi.org/10.1111/gwat.12066

Bedekar V, Morway E, Langevin C, Tonkin M (2016) MT3D-USGS version 1: A U.S. geological survey release of MT3DMS updated with new and expanded transport capabilities for use with MODFLOW

Borah T, Bhattacharjya RK (2015) Development of unknown pollution source identification models using GMS ANN–based simulation optimization methodology. J Hazardous, Toxic, Radioact Waste 19:04014034. https://doi.org/10.1061/(ASCE)HZ.2153-5515.0000242

Brown GH, Brooks MC, Wood AL et al (2012) Aquitard contaminant storage and flux resulting from dense nonaqueous phase liquid source zone dissolution and remediation. Water Resour Res 48:1–17. https://doi.org/10.1029/2011WR011141

Brusseau ML, Russo AE, Schnaar G (2012) Nonideal transport of contaminants in heterogeneous porous media: 9—impact of contact time on desorption and elution tailing. Chemosphere 89:287–292. https://doi.org/10.1016/j.chemosphere.2012.04.038

Carey GR, Chapman SW, Parker BL, McGregor R (2015) Application of an adapted version of MT3DMS for modeling back-diffusion remediation timeframes. Remediat J 25:55–79. https://doi.org/10.1002/rem.21440

Chapman SW, Parker BL (2005) Plume persistence due to aquitard back diffusion following dense nonaqueous phase liquid source removal or isolation. Water Resour Res 41:1–16. https://doi.org/10.1029/2005WR004224

Comunian A, Giudici M (2021) Improving the robustness of the comparison model method for the identification of hydraulic transmissivities. Comput Geosci 149:104705. https://doi.org/10.1016/j.cageo.2021.104705

Elshall AS, Ye M, Finkel M (2020) Evaluating two multi-model simulation–optimization approaches for managing groundwater contaminant plumes. J Hydrol 590:125427. https://doi.org/10.1016/j.jhydrol.2020.125427

Gao G, Feng S, Zhan H et al (2009) Evaluation of anomalous solute transport in a large heterogeneous soil column with mobile-immobile model. J Hydrol Eng 14:966–974. https://doi.org/10.1061/(ASCE)HE.1943-5584.0000071

Gao G, Zhan H, Feng S et al (2010) A new mobile-immobile model for reactive solute transport with scale-dependent dispersion. Water Resour Res 46:1–16. https://doi.org/10.1029/2009WR008707

Guleria A, Chakma S (2022) Mathematical modeling of contaminant transport in the subsurface environment. In: Gupta PK, Yadav B, Himanshu S (eds) Advances in remediation techniques for polluted soils and groundwater. Elsevier, First, pp 141–169

Guleria A, Swami D, Joshi N, Sharma A (2020) Application of temporal moments to interpret solute transport with time-dependent dispersion. Sādhanā 45:159. https://doi.org/10.1007/s12046-020-01402-5

Guleria A, Swami D, Sharma A, Sharma S (2019) Non-reactive solute transport modelling with time-dependent dispersion through stratified porous media. Sādhanā 44:81. https://doi.org/10.1007/s12046-019-1056-6

Guo Z, Brusseau ML (2017a) The impact of well-field configuration and permeability heterogeneity on contaminant mass removal and plume persistence. J Hazard Mater 333:109–115. https://doi.org/10.1016/j.jhazmat.2017.03.012

Guo Z, Brusseau ML (2017b) The impact of well-field configuration on contaminant mass removal and plume persistence for homogeneous versus layered systems. Hydrol Process 31:4748–4756. https://doi.org/10.1002/hyp.11393

Guo Z, Brusseau ML, Fogg GE (2019) Determining the long-term operational performance of pump and treat and the possibility of closure for a large TCE plume. J Hazard Mater 365:796–803. https://doi.org/10.1016/j.jhazmat.2018.11.057

Hughes JD, Langevin CD, Banta E (2017) Documentation for the MODFLOW 6 framework

Kheirabadi M (2018) Groundwater model parameter estimation with simultaneous and sequential use of hydraulic head and travel time measurements

Langevin CD, Hughes JD, Banta ER, et al (2017) Documentation for The MODFLOW 6 groundwater flow model

Leichombam S, Bhattacharjya RK (2019) New hybrid optimization methodology to identify pollution sources considering the source locations and source flux as unknown. J Hazardous, Toxic, Radioact Waste 23:04018037. https://doi.org/10.1061/(ASCE)HZ.2153-5515.0000431

Mescher L (2018) Evaluating the applicability of MODFLOW2005 plus MT3D-USGS: Borden Case Study

Morway ED, Langevin CD, Hughes JD (2021) Use of the MODFLOW 6 water mover package to represent natural and managed hydrologic connections. Groundwater 59:913–924. https://doi.org/10.1111/gwat.13117

Müller S, Schüler L (2019) GeoStat-Framework/GSTools: Reverberating Red v1.1.0

Provost AM, Langevin CD, Hughes JD (2017) Documentation for the " XT3D " option in the node property flow (NPF) package of MODFLOW 6

Rao GT, Rao VVSG, Ranganathan K et al (2011) Assessment of groundwater contamination from a hazardous dump site in Ranipet, Tamil Nadu, India. Hydrogeol J 19:1587–1598. https://doi.org/10.1007/s10040-011-0771-9

Rao GT, Rao VVSG, Surinaidu L et al (2013) Application of numerical modeling for groundwater flow and contaminant transport analysis in the basaltic terrain, Bagalkot, India. Arab J Geosci 6:1819–1833. https://doi.org/10.1007/s12517-011-0461-x

Rasa E, Chapman SW, Bekins BA et al (2011) Role of back diffusion and biodegradation reactions in sustaining an MTBE/TBA plume in alluvial media. J Contam Hydrol 126:235–247. https://doi.org/10.1016/j.jconhyd.2011.08.006

Rezaei A, Zare M, Zhan H (2016) Aquitard horizontal dispersion on reactive solute transport in an aquifer-aquitard system. Transp Porous Media 113:695–716. https://doi.org/10.1007/s11242-016-0719-6

Sathe SS, Mahanta C (2019) Groundwater flow and arsenic contamination transport modeling for a multi aquifer terrain: assessment and mitigation strategies. J Environ Manage 231:166–181. https://doi.org/10.1016/j.jenvman.2018.08.057

Sbai MA (2020) Unstructured gridding for MODFLOW from prior groundwater flow models: a new paradigm. Groundwater 58:gwat.13025. https://doi.org/10.1111/gwat.13025

Sharma PK, Shukla SK, Choudhary R, Swami D (2016) Modeling for solute transport in mobile–immobile soil column experiment. ISH J Hydraul Eng 22:204–211. https://doi.org/10.1080/09715010.2016.1155181

Singh P, Singh RM (2019) Identification of pollution sources using artificial neural network (ANN) and multilevel breakthrough curve (BTC) characterization. Environ Forensics 20:219–227. https://doi.org/10.1080/15275922.2019.1629548

Singh RM, Datta B (2007) Artificial neural network modeling for identification of unknown pollution sources in groundwater with partially missing concentration observation data. Water Resour Manag 21:557–572. https://doi.org/10.1007/s11269-006-9029-z

Singh RM, Datta B (2006) Identification of groundwater pollution sources using GA-based linked simulation optimization model. J Hydrol Eng 11:101–109. https://doi.org/10.1061/(ASCE)1084-0699(2006)11:2(101)

Singh RM, Datta B, Jain A (2004) Identification of unknown groundwater pollution sources using artificial neural networks. J Water Resour Plan Manag 130:506–514. https://doi.org/10.1061/(ASCE)0733-9496(2004)130:6(506)

Sudicky EA (1989) The Laplace Transform Galerkin Technique: a time-continuous finite element theory and application to mass transport in groundwater. Water Resour Res 25:1833–1846. https://doi.org/10.1029/WR025i008p01833

Swami D, Sharma PK, Ojha CSP et al (2018) Asymptotic behavior of mass transfer for solute transport through stratified porous medium. Transp Porous Media 124:699–721. https://doi.org/10.1007/s11242-018-1090-6

Swami D, Sharma PK, Ojha CSP (2016) Behavioral study of the mass transfer coefficient of nonreactive solute with velocity, distance, and dispersion. J Environ Eng 143:1–10. https://doi.org/10.1061/(ASCE)EE.1943-7870.0001164

Vetrimurugan E, Senthilkumar M, Elango L (2017) Solute transport modelling for assessing the duration of river flow to improve the groundwater quality in an intensively irrigated deltaic region. Int J Environ Sci Technol 14:1055–1070. https://doi.org/10.1007/s13762-016-1211-0

White JT, Hemmings B, Fienen MN, Knowling MJ (2021) Towards improved environmental modeling outcomes: enabling low-cost access to high-dimensional, geostatistical-based decision-support analyses. Environ Model Softw 139:105022. https://doi.org/10.1016/j.envsoft.2021.105022

Winston RB (2009) ModelMuse: a graphical user interface for MODFLOW-2005 and PHAST: U.S. geological survey techniques and methods 6–A29. US Geological Survey Reston, VA

Yang M, Annable MD, Jawitz JW (2017a) Forward and back diffusion through argillaceous formations. Water Resour Res 53:4514–4523. https://doi.org/10.1002/2016WR019874

Yang M, Annable MD, Jawitz JW (2017b) Field-scale forward and back diffusion through low-permeability zones. J Contam Hydrol 202:47–58. https://doi.org/10.1016/j.jconhyd.2017.05.001

Yang M, Annable MD, Jawitz JW (2015) Back diffusion from thin low permeability zones. Environ Sci Technol 49:415–422. https://doi.org/10.1021/es5045634

Yang M, McCurley KL, Annable MD, Jawitz JW (2019) Diffusion of solutes from depleting sources into and out of finite low-permeability zones. J Contam Hydrol 221:127–134. https://doi.org/10.1016/j.jconhyd.2019.01.005

Zhan H (1998) Transport of waste leakage in stratified formations. Adv Water Resour 22:159–168. https://doi.org/10.1016/S0309-1708(98)00001-3

Zhan H, Wen Z, Gao G (2009) An analytical solution of two-dimensional reactive solute transport in an aquifer-aquitard system. Water Resour Res 45:1–8. https://doi.org/10.1029/2008WR007479

Zheng C, Bianchi M, Gorelick SM (2011) Lessons learned from 25 years of research at the MADE site. Ground Water 49:649–662. https://doi.org/10.1111/j.1745-6584.2010.00753.x

Zheng C, Wang PP (1999) MT3DMS: a modular three-dimensional multispecies transport model for simulation of advection, dispersion, and chemical reactions of contaminants in groundwater systems